hep-ex/0706.2030

SLAC-PUB-12569
BABAR-TALK-07/041

Hot Topics from the *BABAR* Experiment

A. V. Gritsan
Johns Hopkins University, Baltimore, Maryland 21218, USA

With a sample of about 384 million $B\overline{B}$ pairs recorded with the *BABAR* detector, we search for the flavor-changing charged current transition $B^{\pm} \to \tau^{\pm}\nu$ and perform an amplitude analysis of the effective flavor-changing neutral current transition $B^{\pm} \to \varphi(1020)K^*(892)^{\pm}$. We also extend our search for other K^* final states in the decay $B^0 \to \varphi(1020)K^{*0}$ with a large $K^{*0} \to K^+\pi^-$ invariant mass. Two samples of events with one reconstructed hadronic B decay or one reconstructed semileptonic B decay are selected, and in the recoil a search for $B^{\pm} \to \tau^{\pm}\nu$ is performed. We find a 2.6 σ (3.2 σ not including expected background uncertainty) excess in data which can be converted to a preliminary branching fraction central value of $\mathcal{B}(B^{\pm} \to \tau^{\pm}\nu) = (1.20^{+0.40+0.29}_{-0.38-0.30} \pm 0.22) \times 10^{-4}$. With the decay $B^{\pm} \to \varphi(1020)K^*(892)^{\pm}$, twelve parameters are measured, where our measurements of $f_L = 0.49 \pm 0.05 \pm 0.03$, $f_{\perp} = 0.21 \pm 0.05 \pm 0.02$, and the strong phases point to the presence of a substantial helicity-plus amplitude from a presently unknown source.

1. Introduction

Until the new frontier energy is available at the LHC collider, the Standard Model is being investigated in detail via the rich flavor structure of the quarks and leptons. The study of rare processes, such as flavor-changing neutral and charged currents, already provides constraints on new physics and will allow us to disentangle the flavor structure of particles at the new energy scale once LHC energy is accessible. Until 2008, flavor physics of the third-generation particles, such as b-quark, offers best prospects for discoveries. For example, virtual "loop" transitions of the B meson involve the heaviest presently known particles in the FCNC loop and may reveal new particles through subtle effects. In this paper, we report the most recent ("hot") results on two rare processes $B^{\pm} \to \tau^{\pm}\nu$ and $B^{\pm} \to \varphi(1020)K^*(892)^{\pm}$ with the *BABAR* detector.

In the Standard Model (SM), the purely leptonic decay $B^{\pm} \to \tau^{\pm}\nu$ proceeds via quark annihilation into a W^+ boson, as shown in Fig. 1. The branching fraction is given by:

$$\mathcal{B}(B^+ \to \tau^+\nu) = \frac{G_F^2 m_B m_\tau^2}{8\pi}\left[1 - \frac{m_\tau^2}{m_B^2}\right]^2 \tau_{B^+} f_B^2 |V_{ub}|^2, \quad (1)$$

where V_{ub} is a quark mixing matrix element [1, 2], f_B is the B meson decay constant, G_F is the Fermi constant, τ_{B^+} is the B^+ lifetime, and m_B and m_τ are the B^+ meson and τ masses. Physics beyond the SM, such as two-Higgs doublet models, could enhance or suppress $\mathcal{B}(B^+ \to \tau^+\nu_\tau)$ through the introduction of a charged Higgs boson [3–5], see Fig. 2. Branching fraction in Eq. (1) is modified by a factor:

$$\left[1 - \tan^2\beta \, \frac{m_{B^+}^2}{m_{H^+}^2}\right]^2 , \quad (2)$$

where $\tan\beta$ is the ratio of vacuum expectation values of the two Higgs doublets. Using theoretical calculations of f_B from lattice QCD and experimental measurements of $|V_{ub}|$ from semileptonic B decays, this purely leptonic B-decay can be used to constrain the

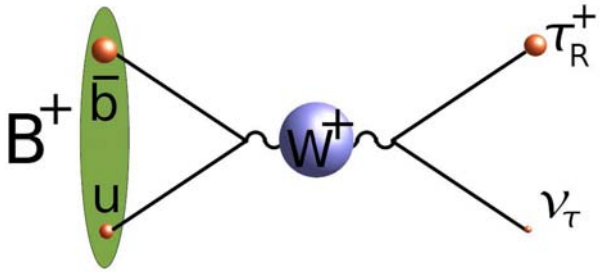

Figure 1: Feynman diagram describing the $B^+ \to \tau^+\nu_\tau$ decay.

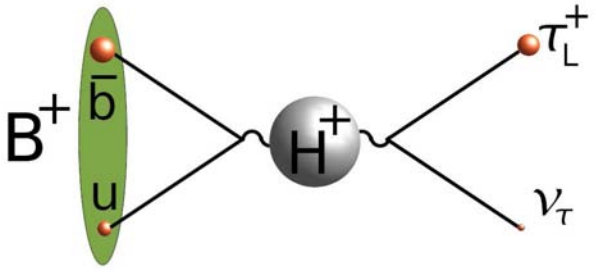

Figure 2: Feynman diagram with potential charged Higgs contribution to the $B^+ \to \tau^+\nu_\tau$ decay.

Invited talk presented at the 5th Flavor Physics And CP Violation Conference (FPCP 2007), 12-16 May 2007, Bled, Slovenia

Work supported in part by US Department of Energy contract DE-AC02-76SF00515

parameters of theories beyond the SM. Or, assuming that SM processes dominate and using the value of $|V_{ub}|$ determined from semileptonic B-decays, purely leptonic decays provide a clean experimental method of measuring f_B precisely.

The branching fractions for $B^+ \to \mu^+\nu$ and $B^+ \to e^+\nu$ are suppressed by factors of $\sim 5 \times 10^{-3}$ and $\sim 10^{-7}$ with respect to $B^+ \to \tau^+\nu_\tau$. The SM estimate of the branching fraction for $B^+ \to \tau^+\nu_\tau$, using $|V_{ub}| = (4.31 \pm 0.30) \times 10^{-3}$ [6] and $f_B = 0.216 \pm 0.022$ GeV [7] in Eq. 1 is $(1.6 \pm 0.4) \times 10^{-4}$. However, a search for $B^+ \to \tau^+\nu_\tau$ is experimentally challenging due to the large missing momentum from multiple neutrinos, which makes the signature less distinctive than in the other leptonic modes. In a previously published analysis using a sample of 223×10^6 $\Upsilon(4S)$ decays, the *BABAR* collaboration set an upper limit of $\mathcal{B}(B^+ \to \tau^+\nu_\tau) < 1.8 \times 10^{-4}$ at the 90% confidence level (CL) [8]. The Belle Collaboration has reported evidence from a search for this decay where the branching fraction was measured to be $\mathcal{B}(B^+ \to \tau^+\nu_\tau) = (1.79^{+0.56}_{-0.49}(\text{stat.})^{+0.46}_{-0.51}(\text{syst})) \times 10^{-4}$ [9].

A vector-vector B-meson decay, such as $B \to \varphi K^*$, is characterized by three complex helicity amplitudes $A_{1\lambda}$ which correspond to helicity states $\lambda = -1, 0, +1$ of the vector mesons. The A_{10} amplitude is expected to dominate [10] due to the $(V - A)$ nature of the weak interactions and helicity conservation in the strong interactions, see Fig. 3. A large fraction of transverse polarization observed by *BABAR* and confirmed by Belle, along with more recent measurements of polarization in rare vector-vector B meson decays $B \to \phi K^*$ and ρK^*, indicate a significant departure from the expected predominance of the longitudinal amplitude [11–15]. The rate, polarization, and *CP* measurements of B meson decays to particles with nonzero spin are sensitive to both strong and weak interaction dynamics and are discussed in a recent review [6, 16].

The polarization anomaly in vector-vector B meson decays suggests other contributions to the decay amplitude, previously neglected. This has motivated a number of proposed contributions from physics beyond the standard model [17]. Depending on New Physics model, hierarchy of decay amplitudes could be modified, as shown in Fig. 4. In addition, there are new mechanisms within the standard model which have been proposed to address the anomaly, such as annihilation penguin [18] or electroweak penguin, or QCD rescattering [19],

In order to distinguish the models, the *BABAR* experiment extended the study of the $B^0 \to \phi K^{*0}$ decays with the tensor ($J^P = 2^+$), vector ($J^P = 1^-$), and scalar ($J^P = 0^+$) K^{*0} [15]. The vector-tensor results are in agreement with quark spin-flip suppression [10] and A_0 amplitude dominance, whereas the vector-vector mode contains substantial A_{+1} amplitude, corresponding to anomalously large transverse polarization.

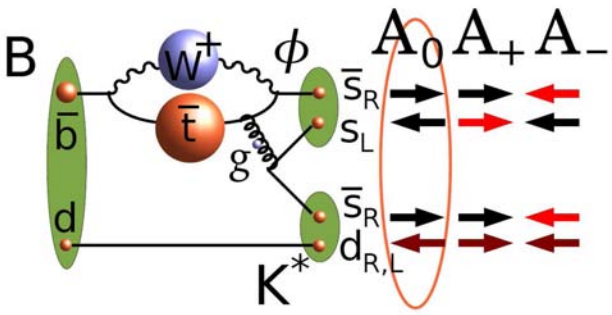

Figure 3: Feynman diagram describing the $B \to \varphi K^*$ decay. Due to the $(V - A)$ nature of the weak interactions, helicity conservation in the strong interactions, and quark-spin suppression shown in the diagram, we expect the hierarchy $A_0 \gg A_{+1} \gg A_{-1}$.

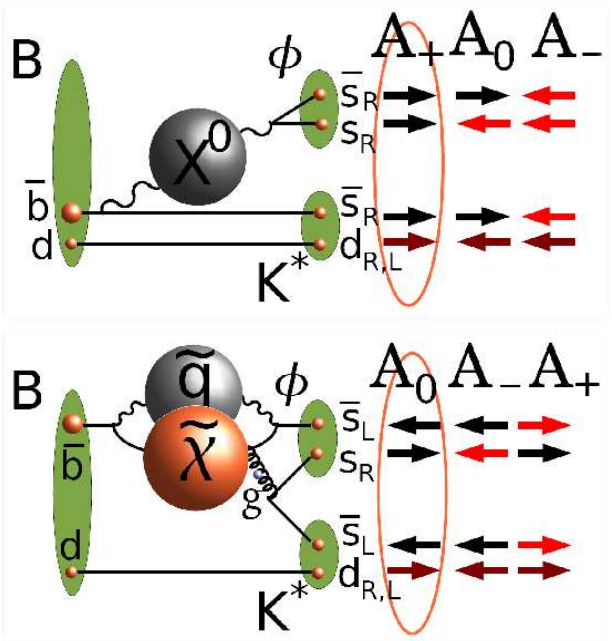

Figure 4: Feynman diagram describing the $B \to \varphi K^*$ decay. Scalar interaction may modify the hierarchy to $A_{+1} \gg A_0 \gg A_{-1}$, while supersymmetric interaction with $(V + A)$ couplings could produce $A_0 \gg A_{-1} \gg A_{+1}$.

We now investigate the polarization puzzle with a full amplitude analysis of the $B^\pm \to \varphi K^*(892)^\pm$ decay. In this paper, we report twelve independent parameters for the three B^+ and three B^- decay amplitudes, six of which are presented for the first time. Moreover, we use the dependence on the $K\pi$ invariant mass of the interference between the $J^P = 1^-$ and 0^+ $(K\pi)^\pm$ components [15, 20, 21] to resolve the discrete ambiguity between the A_{1+1} and A_{1-1} helicity amplitudes.

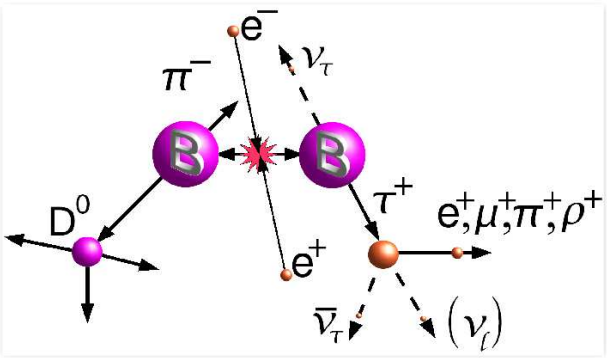

Figure 5: Diagram of he $B^{\pm} \to \tau^{\pm}\nu$ reconstruction technique.

2. The *BABAR* Detector

We use a sample of 383.6 ± 4.2 million $\Upsilon(4S) \to B\overline{B}$ events collected with the *BABAR* detector [22] at the PEP-II e^+e^- asymmetric-energy storage rings. The e^+e^- center-of-mass energy $\sqrt{s}$ is equal to 10.58 GeV. The sample corresponds to an integrated luminosity of $346\,\text{fb}^{-1}$ at the $\Upsilon(4S)$ resonance (on-resonance) and $36.3\,\text{fb}^{-1}$ taken at 40 MeV below the $B\bar{B}$ production threshold (off-resonance) which is used to study background from $e^+e^- \to f\bar{f}$ ($f = u, d, s, c, \tau$) continuum events. The detector components used in this analysis are the tracking system composed of a five-layer silicon vertex detector and a 40-layer drift chamber (DCH), the Cherenkov detector for charged π–K discrimination, a CsI calorimeter (EMC) for photon and electron identification, and an 18–layer flux return (IFR) located outside of the 1.5 T solenoidal coil and instrumented with resistive plate chambers for muon and neutral hadron identification. For the most recent 133 fb^{-1} of data, a portion of the resistive plate chambers has been replaced with limited streamer tubes.

A GEANT4-based [23] Monte Carlo (MC) simulation is used to model signal efficiencies and physics backgrounds. The τ lepton decay is modeled using EvtGen [24]. Beam-related background and detector noise from data are overlaid on the simulated events. Simulation samples equivalent to approximately three times the accumulated data are used to model $B\overline{B}$ events, and samples equivalent to approximately 1.5 times the accumulated data are used to model continuum events. We determine selection efficiencies for signal events using a MC simulation where one B^+ meson decays to $\tau^+\nu$, while the other is allowed to decay into any final state.

3. $B^{\pm} \to \tau^{\pm}\nu$

First we discuss the new preliminary analysis of the $B^{\pm} \to \tau^{\pm}\nu$ decay. Due to the presence of multiple neutrinos, the $B^+ \to \tau^+\nu_\tau$ decay mode lacks the kinematic constraints that are usually exploited in B decay searches in order to reject both continuum and $B\overline{B}$ backgrounds. The strategy adopted for this analysis is to reconstruct exclusively the decay of one of the B mesons in the event, referred to as the "tag" B. The remaining particle(s) in the event (the "recoiling system") are assumed to come from the other B and are compared with the signature expected for $B^+ \to \tau^+\nu_\tau$, see Fig. 5. There are two "tag" methods used in this analysis: full reconstruction of a hadronic B meson decay final state or partial reconstruction of a semileptonic decay. We will discuss in detail the new results with the former method and then briefly show updated results of the latter method with slightly improved precision compared to last year. Then we will combine the two results.

3.1. Analysis Method

In order to avoid experimenter bias, the signal region in data is blinded until the final yield extraction is performed. The $B^+ \to \tau^+\nu_\tau$ signal is searched for in both leptonic and hadronic τ decay modes constituting approximately 71% of the total τ decay width: $\tau^+ \to e^+\nu\overline{\nu}$, $\tau^+ \to \mu^+\nu\overline{\nu}$, $\tau^+ \to \pi^+\overline{\nu}$, and $\tau^+ \to \pi^+\pi^0\overline{\nu}$. We do not consider the $\tau^+ \to \pi^+\pi^-\pi^+\overline{\nu}$ mode since we found it to be dominated by background events.

The tag B candidate is reconstructed in the set of hadronic B decay modes $B^- \to D^{(*)0}X^-$ [25], where X^- denotes a system of charged and neutral hadrons with total charge -1, composed of $n_1\pi^{\pm}\, n_2K^{\pm}\, n_3K^0_S\, n_4\pi^0$, where $n_1 + n_2 \leq 5$, $n_3 \leq 2$, and $n_4 \leq 2$.

The selected sample of tag B candidates is used as normalization for the determination of the branching fraction. We reconstruct $D^{*0} \to D^0\pi^0, D^0\gamma$; $D^0 \to K^-\pi^+$,$K^-\pi^+\pi^0$, $K^-\pi^+\pi^-\pi^+$, $K^0_S\pi^+\pi^-$; and $K^0_S \to \pi^+\pi^-$. The kinematic consistency of tag B candidates is checked with two variables, the beam energy-substituted mass $m_{\rm ES} = \sqrt{s/4 - \vec{p}^{\,2}_B}$ and the energy difference $\Delta E = E_B - \sqrt{s}/2$. Here $\sqrt{s}$ is the total energy in the $\Upsilon(4S)$ center-of-mass (CM) frame, and $\vec{p}_B$ and E_B denote, respectively, the momentum and energy of the tag B candidate in the CM frame. The resolution on ΔE is measured to be $\sigma_{\Delta E} = 10 - 35\,\text{MeV}$, depending on the decay mode, and we require $|\Delta E| < 3\sigma_{\Delta E}$. For each reconstructed B decay mode, its purity $\mathcal{P}$ was estimated as the ratio of the number of peaking events with $m_{\rm ES} > 5.27\,\text{GeV}/c$ to the total number of events in the same range, and is evaluated on on-resonance data. In the event of multiple tag B candidates being reconstructed, the one with the best purity $\mathcal{P}$ is selected.

The background consists of $e^+e^- \to q\bar{q}$ ($q = u, d, s, c$) events and of other $\Upsilon(4S) \to B^0\overline{B}^0$ or

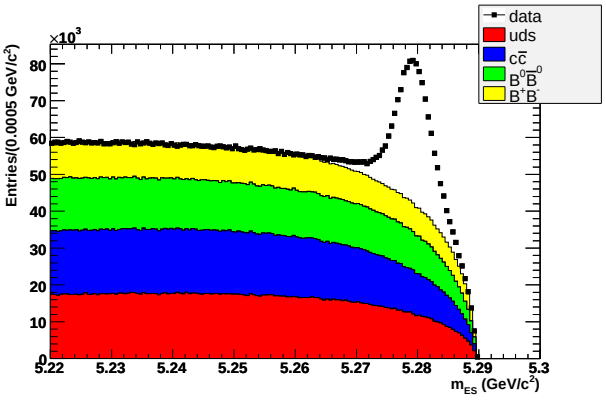

Figure 6: Cumulative distribution of the energy substituted mass $m_{\rm ES}$ of the tag B candidates in data. The non peaking background components are added one on top of the other. From top to bottom are B^+B^-, $B^0\bar{B}^0$, uds and $c\bar{c}$.

B^+B^- decays, in which the tag B candidate is mistakenly reconstructed from particles coming from both B mesons in the event. To significantly reduce the $e^+e^- \to q\bar{q}$ background we require the angle θ^*_{TB}, defined in the CM frame, between the thrust axis [26] of the tag B candidate and the thrust axis of all the charged and neutral reconstructed candidates in the event excluding the ones that form the B^+, to satisfy the requirement $|\cos\theta^*_{TB}| < 0.9$.

In order to determine the number of correctly reconstructed B^+ we classify the background events in four categories: $e^+e^- \to c\bar{c}$; $e^+e^- \to u\overline{u}$, $d\overline{d}$, $s\overline{s}$; $B^0\overline{B}^0$; and B^+B^-. The shapes of these background distributions are taken from MC simulation. The normalizations of the $e^+e^- \to c\bar{c}$ and $e^+e^- \to u\overline{u}$, $d\overline{d}$, $s\overline{s}$ backgrounds are taken from off-resonance data, scaled by the luminosity. The normalization of the $B^0\overline{B}^0$, B^+B^- components are instead obtained by means of a χ^2 fit to the $m_{\rm ES}$ distribution in a sideband region ($5.22\,{\rm GeV}/c^2 < m_{\rm ES} < 5.26\,{\rm GeV}/c^2$). The background contamination in the signal region ($m_{\rm ES} > 5.27\,{\rm GeV}/c^2$) is extrapolated from the fit and subtracted from the data. We estimate the total number of tagged B's in the data as $N_B = (5.92 \pm 0.11_{\rm stat.}) \times 10^5$. Fig. 6 shows the tag B candidate $m_{\rm ES}$ distribution in data compared with MC, and the obtained background subtracted $m_{\rm ES}$ distributions in data.

After the reconstruction of the tag B meson, a selection is applied on the recoiling system in order to enhance the sensitivity to $B^+ \to \tau^+\nu_\tau$ decays. We require the presence of a well reconstructed charged track (signal track) with electric charge opposite to the tag B. The signal track is required to have at least 12 hits in the DCH, its momentum transverse to the beam axis, $p_{\rm T}$, is required to be greater than $0.1\,{\rm GeV}/c$, and its point of closest approach to the interaction point must be less than 10.0 cm along the beam axis and less than 1.5 cm transverse to it.

The τ lepton is identified in the four decay modes: $\tau^+ \to e^+\nu\overline{\nu}$, $\tau^+ \to \mu^+\nu\overline{\nu}$, $\tau^+ \to \pi^+\overline{\nu}$, and $\tau^+ \to \pi^+\pi^0\overline{\nu}$. Particle identification criteria on the signal track are used to separate the four categories. The $\tau^+ \to \pi^+\pi^0\overline{\nu}$ sample is obtained by associating the signal track, identified as pion, to a π^0 reconstructed from a pair of neutral clusters with invariant mass between 0.115 and 0.155 GeV/c^2 and total energy greater than 250 MeV. In case of multiple $\pi^+\pi^0$ candidates the one with largest momentum $p^*_{\pi^+\pi^0}$ is chosen.

Most of the background due to continuum events and incorrectly reconstructed tag B candidates (combinatorial) is rejected by requiring a mode dependent cut on $|cos\theta^*_{TB}|$. Most of the remaining sources of background consists of B^+B^- events in which the tag B meson was correctly reconstructed and the recoil contains one track and additional particles which are not reconstructed by the tracking detectors and calorimeter. From MC simulation we observe that most of this background is from semileptonic B decays.

We define the discriminating variable $E_{\rm extra}$ as the sum of the energies of the neutral clusters not associated with the tag B or with the signal π^0 of the $\tau^+ \to \pi^+\pi^0\overline{\nu}$ mode. For neutral clusters contributing to $E_{\rm extra}$ we need to determine mode-dependent minimum energy thresholds, shown in Table I, in order to ensure a good data-MC agreement at the preselection level, which is a looser selection using only particle identification criteria and a moderate cut on the candidate's momentum. Signal events tend to peak at low $E_{\rm extra}$ values whereas background events, which contain additional sources of neutral clusters, are distributed toward higher $E_{\rm extra}$ values.

Table I EMC barrel and EMC endcap minimum cluster energies (MeV) for electrons, muons and pions samples

Sample	barrel	endcap
electrons	65	70
muons	50	55
pions	50	70

Other variables used to discriminate between signal and background are the CM momentum of the signal candidates, the multiplicity of extra charged track(s) and π^0(s) in the recoil and the direction of the missing momentum four-vector in the CM frame. For the $\tau^+ \to \pi^+\pi^0\overline{\nu}$ mode we exploit the presence of the π^0 in the final state and the dominance of the decay through the ρ resonance by means of the combined quantity s_ρ:

$$s^2_\rho = \left(\frac{m_{\pi\pi^0} - m^{PDG}_\rho}{\Gamma^{PDG}_\rho}\right)^2 + \left(\frac{m_{\gamma\gamma} - m^{PDG}_{\pi^0}}{\sigma_{\pi^0}}\right)^2 \qquad (3)$$

where $m_{\pi\pi^0}$ is the reconstructed invariant mass of the $\pi^+\pi^0$ candidate, $m_{\gamma\gamma}$ is the the reconstructed invariant mass of the π^0 candidate, m_ρ^{PDG} and Γ_ρ^{PDG} are the nominal values [6] for the ρ mass and width, $m_{\pi^0}^{PDG}$ is the nominal π^0 mass and $\sigma_{\pi^0} = 8$ MeV is the experimental resolution on the π^0 mass determined from data.

We optimize the selection on the B^+B^- MC and signal MC for the best $s/\sqrt{s+b}$, where s is the expected signal and b is the expected background from B^+B^- events, in the hypothesis of a branching fraction of 1×10^{-4}, for each mode separately. The optimization procedure is performed simultaneously on all the discriminating variables in order to take into account any correlations. For each discriminating variable α_i we choose a discrete number N_{α_i} of possible selection criteria. We build N= $N_{\alpha_1} \times N_{\alpha_2} \times ....N_{\alpha_k}$ possible selections by combining all the possible cut values for different variables. We include $E_{\rm extra}$ in the optimization, which defines the optimal signal window. We choose the selection corresponding to the best value of $s/\sqrt{s+b}$. The optimized selection criteria are reported in Table II.

Table II Selection criteria optimized for each τ decay mode.

Variable	$e^+\nu\nu$	$\mu^+\nu\nu$	$\pi^+\bar{\nu}$	$\pi^+\pi^0\bar{\nu}$
$E_{\rm extra}$ (GeV)	< 0.160	< 0.100	< 0.230	< 0.290
π^0 multiplicity	0	0	≤ 2	n.a.
Track multipl.	1	1	≤ 2	1
$\lvert cos\theta^*_{TB}\rvert$	≤ 0.9	≤ 0.9	≤ 0.7	≤ 0.7
$p^*_{\rm trk}$(GeV/c)	< 1.25	< 1.85	> 1.5	n.a.
$cos\theta^*_{\rm miss}$	< 0.9	n.a	< 0.5	< 0.55
$p^*_{\pi^+\pi^0}$(GeV/c)	n.a.	n.a.	n.a.	> 1.5
ρ quality	n.a.	n.a.	n.a.	< 2.0
E_{π^0} (GeV)	n.a.	n.a.	n.a.	> 0.250

We compute the efficiency as the ratio of the number of signal MC events passing the selection criteria and the number of events that have a $m_{\rm ES}$ peaking tag B candidate, in the signal region $m_{\rm ES} > 5.27\,{\rm GeV}$. We evaluate the efficiencies on a signal MC sample which is distinct from the sample used in the optimization procedure. A small cross-feed is present in some modes and it is taken into account in the computation of the total efficiency.

The total efficiency for each selection is:

$$\varepsilon_i = \sum_{j=1}^{n_{dec}} \varepsilon_i^j f_j \ , \qquad (4)$$

where ε_i^j is the efficiency of the selection i for the τ decay mode j, $n_{\rm dec} = 7$ is the number of of τ decay modes and f_j are the fractions of the τ decay mode as estimated from the signal MC sample with a reconstructed B. Table III shows the estimated efficiencies.

Table III Selection efficiency (%) for the τ decay modes. The last row shows the total efficiency including small cross-feed from other τ decays (not shown explicitly) and weighted by the decay abundance at the tag selection level. The errors are statistical only. Note that mode dependent $E_{\rm extra}$ selection is applied as reported in Table II.

$\tau^+ \to e^+\nu\overline{\nu}$	19.3 ± 1.1
$\tau^+ \to \mu^+\nu\overline{\nu}$	10.8 ± 0.9
$\tau^+ \to \pi^+\overline{\nu}$	19.7 ± 1.3
$\tau^+ \to \pi^+\pi^0\overline{\nu}$	7.0 ± 0.5
Total:	9.8 ± 0.3

In order to determine the expected number of background events in the data, we use the final selected data samples with $E_{\rm extra}$ between 0 and 2.4 GeV.

We first perform an extended unbinned maximum likelihood fit to the $m_{\rm ES}$ distribution in the final sample, in the $E_{\rm extra}$ sideband region $0.4\,{\rm GeV} < E_{\rm extra} < 2.4\,{\rm GeV}$. We use as probability density function(PDF) for the peaking component a Gaussian function joined to an exponential tail (Crystal Ball), and as a PDF for the non peaking component a phase space motivated threshold function [27] (Argus). From this fit, we determine a peaking yield $N_{pk}^{\rm high,data}$ and signal shape parameters, to be used in later fits. We apply the same procedure on B^+B^- MC events which pass the final selection and determine the peaking yield $N_{pk}^{\rm high,MC}$. By fitting $m_{\rm ES}$ in the $E_{\rm extra}$ signal region (with the Crystal Ball parameters fixed to the values determined in the $E_{\rm extra}$ sideband fits) in the MC sample, we determine the MC peaking yield $N_{pk}^{\rm low,MC}$. We perform a similar fit to data in order to extract the amount of combinatorial background n_{comb}, as the integral of the Argus shaped component in the $m_{\rm ES} > 5.27\,{\rm GeV}$ domain.

We estimate the total background prediction in the signal region as:

$$b = N_{pk}^{\rm low,MC} \times \frac{N_{pk}^{\rm high,data}}{N_{pk}^{\rm high,MC}} + n_{comb} \qquad (5)$$

Due to the low statistics of the final selected sample an alternative procedure for estimating the background, which avoids fitting the $m_{\rm ES}$ distribution in the final samples, is also performed. We fit $m_{\rm ES}$ in the preselection samples $E_{\rm extra}$ sideband to determine the combinatorial background yield $N_{comb}^{\rm high,data\ presel}$ and in the low $E_{\rm extra}$ region to determine the amount of combinatorial background in the preselection signal region $n_{comb}^{\rm presel}$. The preselection samples are defined by a looser selection only requiring particle identification for the charged track and a lower bound on the CM momentum of 0.6 GeV/c for the pion candidate and of 1.0 GeV/c for the $\pi^+\pi^0$candidate.

We then fit the $m_{\rm ES}$ distribution in the final samples

in the $E_{\rm extra}$ sideband to determine the combinatorial background yield $N_{comb}^{\rm high,data}$. We estimate the combinatorial background in the low $E_{\rm extra}$ in the final selected sample n_{comb} scaling $n_{comb}^{\rm presel}$ as

$$n_{comb} = n_{comb}^{\rm presel} \times \frac{N_{comb}^{\rm high,data}}{N_{comb}^{\rm high,data\ presel}} \qquad (6)$$

The same procedure is applied to MC to subtract the combinatorial background and determine the MC peaking yield as:

$$N_{pk}^{\rm low,MC} = N_{tot}^{\rm low,MC} - n_{comb}^{\rm MC\ presel} \times \frac{N_{comb}^{\rm high,MC}}{N_{comb}^{\rm high,MC\ presel}} \qquad (7)$$

This peaking component is scaled by the same scale factor $N_{pk}^{\rm high,data}/N_{pk}^{\rm high,MC}$ of the first method and it is added to the combinatorial of Eq. (6) to obtain the background predictions as in Eq. (5).

We use the mean value between the two methods to obtain the final estimate. We determine the error on the estimate by adding in quadrature the statistical error from the first method with the half of the difference between the two values to obtain the total error on the background prediction. The expected numbers of background events in the four reconstructed modes are shown in Table IV.

Table IV The mean value of expected number of background events in the signal region, using method A and method B, respectively. The last column shows the average background prediction used in the likelihood scan to extract the signal branching fraction.

	method A	method B	average
$\tau^+ \to e^+\nu\overline{\nu}$	1.1 ± 0.9	1.9 ± 1.0	1.5 ± 1.4
$\tau^+ \to \mu^+\nu\overline{\nu}$	1.9 ± 1.0	1.6 ± 0.8	1.8 ± 1.0
$\tau^+ \to \pi^+\overline{\nu}$	6.5 ± 2.0	7.1 ± 1.9	6.8 ± 2.1
$\tau^+ \to \pi^+\pi^0\overline{\nu}$	4.1 ± 1.4	4.3 ± 1.3	4.2 ± 1.4
All modes	13.6 ± 2.8	14.9 ± 3.7	14.3 ± 3.0

3.2. Results

After finalizing the signal selection criteria, we measure the yield of events in each decay mode in the signal region of the on-resonance data. Table V lists the number of observed events in on-resonance data in the signal region, together with the expected number of background events in the signal region. Figs. 7 and 8 show the $E_{\rm extra}$ distribution for data and expected background at the end of the selection. The signal MC, scaled to a branching fraction $\mathcal{B}(B^+ \to \tau^+\nu_\tau) = 10^{-3}$ is overlaid for comparison. The $E_{\rm extra}$ distribution is also plotted separately for each τ decay mode.

We determine the $B^+ \to \tau^+\nu_\tau$ branching fraction from the number of fitted signal candidates s in data

Table V The observed number of on-resonance data events in the signal region is shown, together with the mean number of expected background events.

τ decay mode	background	Observed
$\tau^+ \to e^+\nu\overline{\nu}$	1.47 ± 1.37	4
$\tau^+ \to \mu^+\nu\overline{\nu}$	1.78 ± 0.97	5
$\tau^+ \to \pi^+\overline{\nu}$	6.79 ± 2.11	10
$\tau^+ \to \pi^+\pi^0\overline{\nu}$	4.23 ± 1.39	5
All modes	14.27 ± 3.03	24

according to:

$$\mathcal{B}(B^+ \to \tau^+\nu_\tau) = \frac{\varepsilon_B^{\rm tag}}{\varepsilon_{\rm sig}^{\rm tag}} \times \frac{s}{\varepsilon_{\tau\nu} N_{B^\pm}^{\rm tag}} \qquad (8)$$

where $N_{B^\pm}^{\rm tag}$ is the number of tag B^+ meson correctly reconstructed, $\varepsilon_B^{\rm tag}$, $\varepsilon_{\rm sig}^{\rm tag}$ are the tag B efficiencies in generic $B\bar{B}$ and signal events respectively, and $\varepsilon_{\tau\nu}$ is the efficiency to select a signal $B \to \tau\nu$ decay in a tagged event. The ratio $r_\varepsilon = \frac{\varepsilon_{\rm sig}^{\rm tag}}{\varepsilon_B^{\rm tag}}$ was determined from MC simulation to be $r_\varepsilon = 0.939 \pm 0.007$.

The results from each of our four signal decay modes

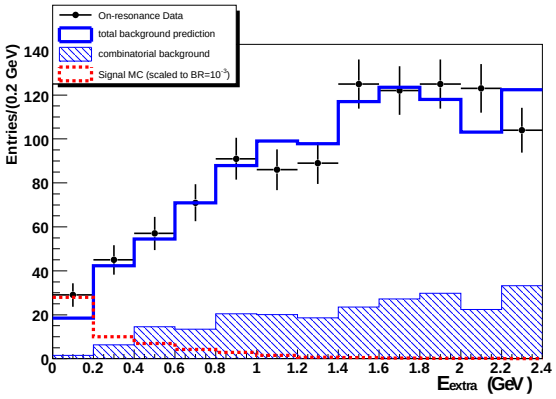

Figure 7: The $E_{\rm extra}$ distribution for all the τ modes combined.

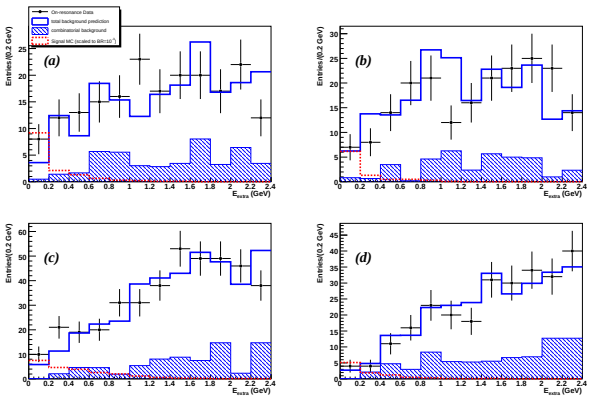

Figure 8: The $E_{\rm extra}$ distribution for the (a) $\tau^+ \to e^+\nu\overline{\nu}$, (b) $\tau^+ \to \mu^+\nu\overline{\nu}$, (c) $\tau^+ \to \pi^+\overline{\nu}$, and (d) $\tau^+ \to \pi^+\pi^0\overline{\nu}$ modes.

(n_{ch}) are combined using the estimator $Q = \mathcal{L}(s+b)/\mathcal{L}(b)$, where $\mathcal{L}(s+b)$ and $\mathcal{L}(b)$ are the likelihood functions for signal plus background and background-only hypotheses, respectively:

$$\mathcal{L}(s+b) \equiv \prod_{i=1}^{n_{ch}} \frac{e^{-(s_i+b_i)}(s_i+b_i)^{n_i}}{n_i!},\ \mathcal{L}(b) \equiv \prod_{i=1}^{n_{ch}} \frac{e^{-b_i} b_i^{n_i}}{n_i!}. \quad (9)$$

where $s_i = \varepsilon_i s$. We include the systematic uncertainties, including those of a statistical nature, on the expected background (b_i) in the likelihood definition by convolving it with a Gaussian function. The mean of the Gaussian is b_i, and the standard deviation (σ_{b_i}) of the Gaussian is the error on b_i [28].

We compute the central value of the branching fraction (including statistical uncertainty and uncertainty from the background) by scanning over signal branching fraction hypotheses between 0.0 and 3.0×10^{-4} in steps of 0.025×10^{-4} and computing the value of $\mathcal{L}(s+b)/\mathcal{L}(b)$ for each hypothesis. The branching fraction is the hypothesis which minimizes $Q = -2\ln(\mathcal{L}(s+b)/\mathcal{L}(b))$, and the statistical uncertainty is determined by finding the points on the likelihood scan that occur at one unit above the minimum. The systematic error is computed for the branching fraction as a fraction of the central value.

The main sources of uncertainty in the determination of the $B^+ \to \tau^+\nu_\tau$ branching fraction come from the estimation of the tag yield and efficiency, the reconstruction efficiency of the signal modes and the number of expected background events. We estimate a systematic uncertainty due to the technique used to determine the tag B yield and reconstruction efficiency, varying the MC based criteria to define the B^+B^- non-peaking component of the $m_{\rm ES}$ shape. Observing the effect due to the different choices on the branching fraction measurement, we assign a systematic uncertainty of 3%. The systematic uncertainty of the signal efficiencies depends on the τ decay mode and includes the effects of the tracking of charged particles, particle identification, and the π^0 reconstruction efficiency. The dominant efficiency uncertainty was found to be due to E_{extra} selection requirement and is found to be 15%. The contributions due to the tracking and to the choice of the E_{extra} selection are treated as correlated among the different channels.

The systematic uncertainty on the background prediction has been estimated using two different methods to extract the combinatorial background, and it has been found to be negligible with respect to the statistical uncertainty. This uncertainty has been incorporated in the likelihood definition used to extract the branching fraction.

We determine the branching fraction central value to be

$$\mathcal{B}(B^+ \to \tau^+\nu_\tau) = 1.8^{+1.0}_{-0.9}(\text{stat+bkg}) \pm 0.3(\text{syst})) \times 10^{-4}. \quad (10)$$

We obtain a significance of 2.7 σ from $\Sigma = \sqrt{\text{Q}_{\rm min}}$, where $\text{Q}_{\rm min}$ is the minimum value of the likelihood ratio, if we do not include the uncertainties on the background predictions. If we include the background uncertainty into account we obtain the smaller significance of 2.2 σ. We compute the 90% C.L. upper limit using the CL_s method [29] to be $\mathcal{B}(B^+ \to \tau^+\nu_\tau) < 3.4 \times 10^{-4}$.

3.3. Combined Results

We report here the branching fraction obtained by combining the hadronic tag analysis result, described in this document, with the *BABAR* semileptonic tag analysis result, based on a statistically independent data sample and reported in [30]. Both the analyses proceed in a similar manner for the four τ decay mode reconstruction and use the same likelihood ratio scan technique to combine the different τ decay modes. Fig. 9 shows the $E_{\rm extra}$ distribution for all the τ modes combined in the analysis with semileptonic tag.

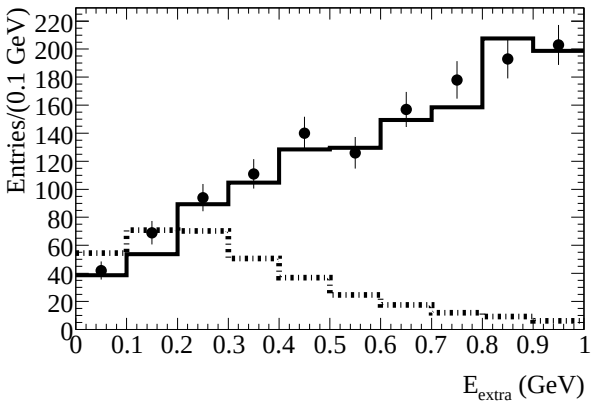

Figure 9: The $E_{\rm extra}$ distribution for all the τ modes combined in the analysis with semileptonic tag. The dashed line shows predicted signal distribution assuming the $B^\pm \to \tau^\pm\nu$ branching fraction of 10^{-3}.

The likelihood ratio is extended to combine eight reconstruction modes, four from the hadronic tag and four from the semileptonic tag. We obtain

$$\mathcal{B}(B^+ \to \tau^+\nu_\tau) = (1.20^{+0.40}_{-0.38}(\text{stat})^{+0.29}_{-0.30}(\text{bkg}) \pm 0.22(\text{syst})) \times 10^{-4}, \quad (11)$$

where the first error is statistical, the second is due to the background prediction systematic uncertainty, and the third one is due to the other systematic sources. We obtain a significance of 2.6 σ including the uncertainty on the expected background (3.2 σ if this uncertainty is not included).

Fig. 10 shows the $\mathcal{L}(s+b)/\mathcal{L}(b)$ scan as a function of signal branching fraction (the background uncertainty is included in the likelihood).

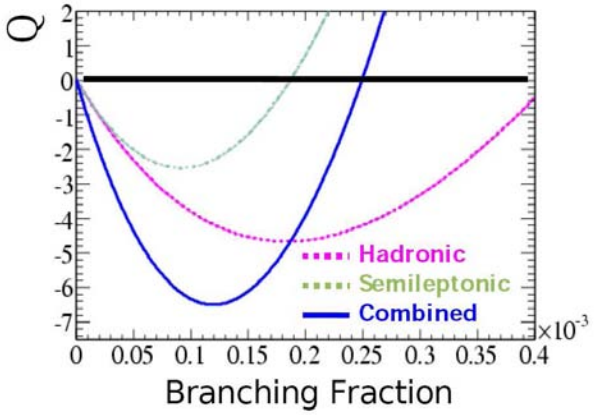

Figure 10: Scan of $Q = -2ln(\mathcal{L}(s+b)/\mathcal{L}(b))$ as a function of the $B^{\pm} \to \tau^{\pm}\nu$ decay branching fraction. The uncertainty on the expected number of background events has been included in the likelihood definition. The results are shown for the hadronic tag, semileptonic tag, and combined analysis.

3.4. Discussion

In summary, we report here preliminary branching fraction of the $B^{\pm} \to \tau^{\pm}\nu$ decay using two independent methods of tag B reconstruction: hadronic and semileptonic B decay in the recoil. We find a 2.6 σ (3.2 σ not including expected background uncertainty) excess in data which can be converted to a preliminary branching fraction central value of $\mathcal{B}(B^{\pm} \to \tau^{\pm}\nu) = (1.20^{+0.40+0.29}_{-0.38-0.30} \pm 0.22) \times 10^{-4}$.

Given the measurement of the $B^{\pm} \to \tau^{\pm}\nu$ branching fraction, we may constraint CKM parameter V_{ub} using Eq. (1). See Fig 11 for illustration. Alternatively, given the best world measurements of parameters present in Eq. (1), we can constraint $\tan\beta$ and charged Higgs mass in the model with two Higgs doublets, as shown in Fig 12.

4. $B^{\pm} \to \varphi(1020)K^*(892)^{\pm}$

One of our goals is to test the quark-spin projections in the $B \to \varphi K^*$ decay, as shown in Fig. 3. However, equivalently we can measure spin projections of the two vector mesons in the B decay. There are three complex amplitudes for the three spin projections possible, and therefore there are a total of 12 non-trivial independent real parameters describing the B and $\overline{B}$ decays. Information about the amplitude sizes and phases can be deduced from analysis of angular distribution as illustrated in Fig. 13.

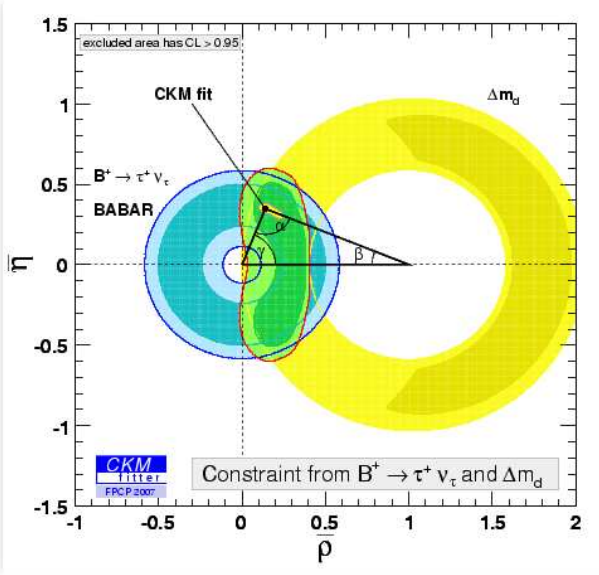

Figure 11: Constraints at 95% C.L. on ρ and η parameters (through measurement of V_{ub}) of the CKM triangle using $B^{\pm} \to \tau^{\pm}\nu$ results presented here, see Eq. (1). Constraints from B_d-mixing are also shown, along with combined results [31].

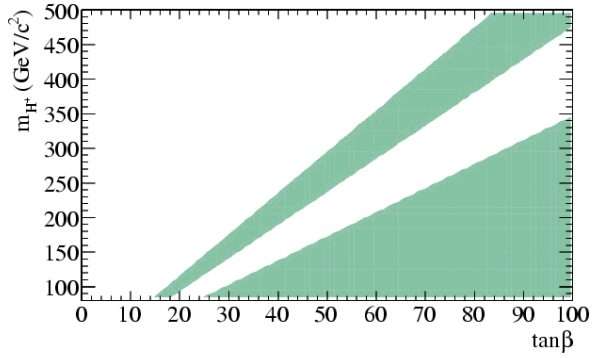

Figure 12: Constraints on $\tan\beta$ and charged Higgs mass from $B^{\pm} \to \tau^{\pm}\nu$ results presented here, see Eqs. (1) and (2). Shaded areas are excluded at 95% C.L.

4.1. Analysis Method

The $B^{\pm} \to \varphi(1020)K^{*\pm} \to (K^+K^-)(K\pi)^{\pm}$ candidates are analyzed with two $(K\pi)^{\pm}$ final states, $K^0_S\pi^{\pm}$ and $K^{\pm}\pi^0$. The neutral pseudoscalar mesons are reconstructed in the final states $K^0_S \to \pi^+\pi^-$ and $\pi^0 \to \gamma\gamma$. We define the helicity angle θ_i as the angle between the direction of the K or K^+ meson from $K^* \to K\pi$ (θ_1) or $\varphi \to K^+K^-$ (θ_2) and the direction opposite the B in the K^* or φ rest frame, and Φ as the angle between the decay planes of the two systems, see Fig. 13. The differential decay width has four complex amplitudes $A_{J\lambda}$ which describe two spin states of the $K\pi$ system ($J = 1$ or 0) and the three

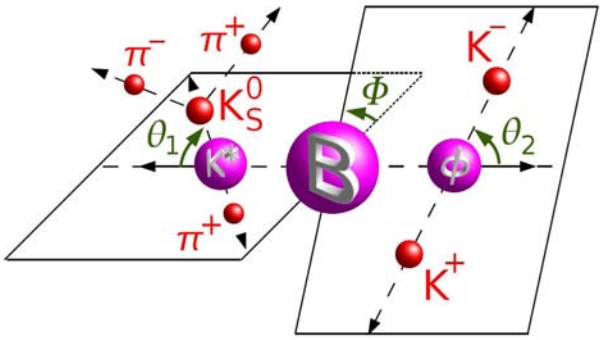

Figure 13: Definition of decay angles given in the rest frames of the decaying parents.

helicity states of the $J = 1$ state ($\lambda = 0$ or ± 1):

$$\frac{d^3\Gamma}{d\mathcal{H}_1 d\mathcal{H}_2 d\Phi} \propto \left| \sum A_{J\lambda} Y_J^{\lambda}(\mathcal{H}_1, \Phi) Y_1^{-\lambda}(-\mathcal{H}_2, 0) \right|^2 \quad (12)$$

where $\mathcal{H}_i = \cos\theta_i$ and Y_J^{λ} are the spherical harmonics with $J = 1$ for $K^*(892)$ and $J = 0$ for $(K\pi)_0^*$. We reparameterize the amplitudes as $A_{1\pm1} = (A_{1\parallel} \pm A_{1\perp})/\sqrt{2}$.

We identify B meson candidates using two kinematic variables: $m_{\rm ES} = [(s/2 + \mathbf{p}_\Upsilon \cdot \mathbf{p}_B)^2/E_\Upsilon^2 - \mathbf{p}_B^2]^{1/2}$ and $\Delta E = (E_\Upsilon E_B - \mathbf{p}_\Upsilon \cdot \mathbf{p}_B - s/2)/\sqrt{s}$, where $(E_B, \mathbf{p}_B)$ is the four-momentum of the B candidate, and $(E_\Upsilon, \mathbf{p}_\Upsilon)$ is the e^+e^- initial state four-momentum, both in the laboratory frame. We require $m_{\rm ES} > 5.25$ GeV and $|\Delta E| < 0.1$ GeV. The requirements on the invariant masses are $0.75 < m_{K\pi} < 1.05$ GeV, $0.99 < m_{K\overline{K}} < 1.05$ GeV, $|m_{\pi\pi} - m_{K^0}| < 12$ MeV, and $120 < m_{\gamma\gamma} < 150$ MeV for the $K^{*\pm}$, φ, K^0_S, and π^0, respectively. For the K^0_S candidates, we also require the cosine of the angle between the flight direction from the interaction point and momentum direction to be greater than 0.995 and the measured proper decay time greater than five times its uncertainty.

To reject the dominant $e^+e^- \to$ quark-antiquark background, we use the angle θ_T between the B-candidate thrust axis and that of the rest of the event, and a Fisher discriminant $\mathcal{F}$ [32]. Both variables are calculated in the center-of-mass frame. The discriminant combines the polar angles of the B-momentum vector and the B-candidate thrust axis with respect to the beam axis, and two moments of the energy flow around the B-candidate thrust axis [32].

To reduce combinatorial background with low-momentum π^0 candidates, we require $\mathcal{H}_1 < 0.6$. When more than one candidate is reconstructed, which happens in 7% of events with K^0_S and 17% with π^0, we select the one whose χ^2 of the charged-track vertex fit combined with χ^2 of the invariant mass consistency of the K^0_S or π^0 candidate, is the lowest. We define the b-quark flavor sign Q to be opposite to the charge of the B meson candidate.

We use an unbinned, extended maximum-likelihood fit [11, 15] to extract the event yields n_j^k and the parameters of the probability density function (PDF) $\mathcal{P}_j^k$. The index j represents three event categories used in our data model: the signal $B^\pm \to \varphi(K\pi)^\pm$ ($j = 1$), a possible background from $B^\pm \to f_0(980)K^{*\pm}$ ($j = 2$), and combinatorial background ($j = 3$). The superscript k corresponds to the value of $Q = \pm$ and allows for a CP-violating difference between the B^+ and B^- decay amplitudes (A and $\overline{A}$). In the signal category, the yield and asymmetry of the $B^\pm \to \varphi K^*(892)^\pm$ mode, $n_{\rm sig}$ and $\mathcal{A}_{CP}$, and those of the $B^\pm \to \varphi(K\pi)_0^{*\pm}$ mode are parameterized by applying the fraction of $\varphi K^*(892)^\pm$ yield, μ^k, to n_1^k. Hence, $n_{\rm sig} = n_1^+ \times \mu^+ + n_1^- \times \mu^-$, $\mathcal{A}_{CP} = (n_1^+ \times \mu^+ - n_1^- \times \mu^-)/n_{\rm sig}$, and the $\varphi(K\pi)_0^{*\pm}$ yield is $n_1^+ \times (1 - \mu^+) + n_1^- \times (1 - \mu^-)$.

The likelihood $\mathcal{L}_i$ for each candidate i is defined as $\mathcal{L}_i = \sum_{j,k} n_j^k \mathcal{P}_j^k(\mathbf{x_i};\, \mu^k,\, \boldsymbol{\zeta},\, \boldsymbol{\xi})$, where the PDF is formed based on the following set of observables $\mathbf{x_i} = \{\mathcal{H}_1,\, \mathcal{H}_2,\, \Phi,\, m_{K\pi},\, m_{K\overline{K}},\, \Delta E,\, m_{\rm ES},\, \mathcal{F},\, Q\}$ and the dependence on μ^k and polarization parameters $\boldsymbol{\zeta}$ is relevant only for the signal PDF $\mathcal{P}_1^k$. The remaining PDF parameters $\boldsymbol{\xi}$ are left free to vary in the fit for the combinatorial background and are fixed to the values extracted from Monte Carlo (MC) simulation [23] and calibration $B \to \overline{D}\pi$ decays for event categories $j = 1$ and 2.

The helicity part of the signal PDF is the ideal angular distribution from Eq. (12), multiplied by an empirical acceptance function $\mathcal{G}(\mathcal{H}_1, \mathcal{H}_2, \Phi) \equiv \mathcal{G}_1(\mathcal{H}_1) \times \mathcal{G}_2(\mathcal{H}_2)$. Here, the amplitudes $A_{J\lambda}$ are expressed in terms of the polarization parameters $\boldsymbol{\zeta} \equiv \{f_L,\, f_\perp,\, \phi_\parallel,\, \phi_\perp,\, \delta_0,\, \mathcal{A}_{CP}^0,\, \mathcal{A}_{CP}^\perp,\, \Delta\phi_\parallel,\, \Delta\phi_\perp,\, \Delta\delta_0\}$ defined in Table VI. CP-violating differences are incorporated via the replacements in Eq. (12) for B^+ decays: $f_L \to f_L \times (1 + \mathcal{A}_{CP}^0 \times Q)$, $f_\perp \to f_\perp \times (1 + \mathcal{A}_{CP}^\perp \times Q)$, $\phi_\parallel \to (\phi_\parallel + \Delta\phi_\parallel \times Q)$, $\phi_\perp \to (\phi_\perp + \pi/2 + (\Delta\phi_\perp + \pi/2) \times Q)$, and $\delta_0 \to (\delta_0 + \Delta\delta_0 \times Q)$.

A relativistic spin-J Breit–Wigner amplitude parameterization is used for the resonance masses [6, 33], and the $(K\pi)_0^{*\pm}$ $m_{K\pi}$ amplitude is parameterized with the LASS function [20]. The latter includes the $K_0^*(1430)^\pm$ resonance together with a nonresonant component. The interference between the $J = 0$ and 1 $(K\pi)^\pm$ contributions is modeled with the three terms $2\mathcal{R}{\rm e}(A_{1\lambda}A_{00}^*)$ in Eq. (12) with the four-dimensional angular and $m_{K\pi}$ parameterization and with dependence on μ^k and $\boldsymbol{\zeta}$.

The signal PDF for a given candidate i is a joint PDF for the helicity angles and resonance mass as discussed above, and the product of the PDFs for each of the remaining variables. The combinatorial background PDF is the product of the PDFs for independent variables and is found to describe well both the dominant quark-antiquark background and the

Table VI Summary of results for the $B^\pm \to \varphi K^*(892)^\pm$ decay. The twelve primary results are presented for the two decay subchannels along with the combined results, where the branching fraction $\mathcal{B}$ is computed using the number of signal events $n_{\rm sig}$ and the total selection efficiency ε, which includes the daughter branching fractions [6] and the reconstruction efficiency $\varepsilon_{\rm reco}$ obtained from MC simulation. The definition of the six *CP*-violating parameters allows for differences between the B^+ and B^- decay amplitudes A and $\overline{A}$ with superscript $Q = -$ and $+$, respectively. The systematic uncertainties are quoted last and are not included for the intermediate primary results in each subchannel. The dominant fit correlation coefficients ($\mathcal{C}$) are presented, where we show correlations of δ_0 with $\phi_\parallel/\phi_\perp$ and of $\Delta\delta_0$ with $\Delta\phi_\parallel/\Delta\phi_\perp$.

parameter	definition	$K^*(892)^\pm \to K^0_S\pi^\pm$	$K^*(892)^\pm \to K^\pm\pi^0$	combined	$\mathcal{C}$
$\mathcal{B}$	$\Gamma/\Gamma_{\rm total}$	$(10.5 \pm 1.4) \times 10^{-6}$	$(11.6 \pm 1.5) \times 10^{-6}$	$(11.2 \pm 1.0 \pm 0.9) \times 10^{-6}$	
f_L	$\lvert A_{10}\rvert^2/\Sigma\lvert A_{1\lambda}\rvert^2$	0.51 ± 0.07	$0.46^{+0.10}_{-0.09}$	$0.49 \pm 0.05 \pm 0.03$	$\}-58\%$
$f_\perp$	$\lvert A_{1\perp}\rvert^2/\Sigma\lvert A_{1\lambda}\rvert^2$	$0.22^{+0.07}_{-0.06}$	$0.21^{+0.09}_{-0.08}$	$0.21 \pm 0.05 \pm 0.02$	
$\phi_\parallel - \pi$	$\arg(A_{1\parallel}/A_{10}) - \pi$	$-0.75^{+0.28}_{-0.24}$	-0.77 ± 0.35	$-0.67 \pm 0.20 \pm 0.07$	$\}+56\%$
$\phi_\perp - \pi$	$\arg(A_{1\perp}/A_{10}) - \pi$	-0.15 ± 0.24	$-0.89^{+0.40}_{-0.46}$	$-0.45 \pm 0.20 \pm 0.03$	
$\delta_0 - \pi$	$\arg(A_{00}/A_{10}) - \pi$	-0.25 ± 0.24	$+0.11 \pm 0.31$	$-0.07 \pm 0.18 \pm 0.06$	$+37\%/+36\%$
$\mathcal{A}_{CP}$	$(\Gamma^+ - \Gamma^-)/(\Gamma^+ + \Gamma^-)$	-0.09 ± 0.13	$+0.07 \pm 0.13$	$0.00 \pm 0.09 \pm 0.04$	
$\mathcal{A}^0_{CP}$	$(f_L^+ - f_L^-)/(f_L^+ + f_L^-)$	$+0.24 \pm 0.15$	$+0.09 \pm 0.20$	$+0.17 \pm 0.11 \pm 0.02$	$\}-50\%$
$\mathcal{A}^\perp_{CP}$	$(f_\perp^+ - f_\perp^-)/(f_\perp^+ + f_\perp^-)$	$+0.12 \pm 0.31$	$+0.41^{+0.54}_{-0.40}$	$+0.22 \pm 0.24 \pm 0.08$	
$\Delta\phi_\parallel$	$(\phi_\parallel^+ - \phi_\parallel^-)/2$	$+0.02 \pm 0.28$	$+0.22 \pm 0.35$	$+0.07 \pm 0.20 \pm 0.05$	$\}+57\%$
$\Delta\phi_\perp$	$(\phi_\perp^+ - \phi_\perp^- - \pi)/2$	$+0.18 \pm 0.24$	$+0.48^{+0.46}_{-0.40}$	$+0.19 \pm 0.20 \pm 0.07$	
$\Delta\delta_0$	$(\delta_0^+ - \delta_0^-)/2$	$+0.13 \pm 0.24$	$+0.34 \pm 0.31$	$+0.20 \pm 0.18 \pm 0.03$	$+37\%/+37\%$
$n_{\rm sig}$		$102 \pm 13 \pm 6$	$117^{+15}_{-16} \pm 7$		
ε		(2.53 ± 0.13) %	(2.59 ± 0.17) %		
$\varepsilon_{\rm reco}$		(22.3 ± 1.2) %	(16.0 ± 1.0) %		

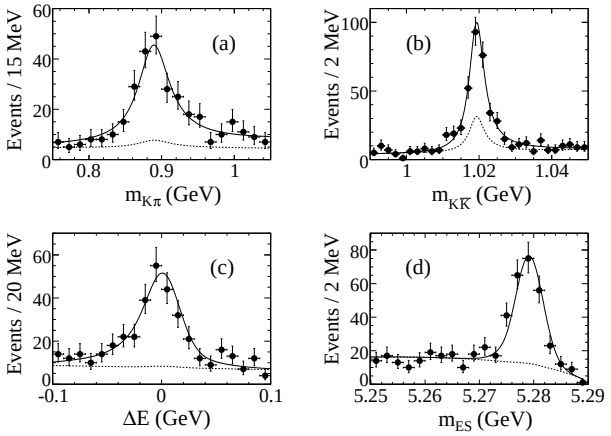

Figure 14: Projections onto the variables (a) $m_{K\pi}$, (b) $m_{K\overline{K}}$, (c) ΔE, and (d) $m_{\rm ES}$ for the signal $B^\pm \to \varphi(K\pi)^\pm$ candidates with a requirement discussed in the text. The solid (dashed) lines show the signal-plus-background (background) PDF projections.

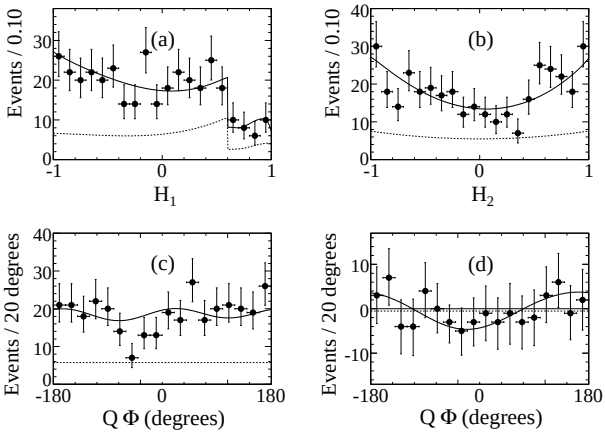

Figure 15: Projections onto the variables (a) $\mathcal{H}_1$, (b) $\mathcal{H}_2$, (c) $Q\,\Phi$, and (d) the differences between the $Q\,\Phi$ projections for events with $\mathcal{H}_1\,\mathcal{H}_2 > 0$ and with $\mathcal{H}_1\,\mathcal{H}_2 < 0$ for the signal $B^\pm \to \varphi(K\pi)^\pm$ candidates following the solid (dashed) line definitions in Fig. 14. The step in the $\mathcal{H}_1$ PDF distributions is due to the selection requirement $\mathcal{H}_1 < 0.6$ in the $B^\pm \to \varphi(K^\pm\pi^0)$ channel.

background from random combinations of B tracks. The signal and background PDFs are illustrated in Figs. 14 and 15. For illustration, the signal fraction is enhanced with a requirement on the signal-to-background probability ratio, calculated with the plotted variable excluded, that is at least 50% efficient for signal $B^\pm \to \varphi(K\pi)^\pm$ events. We use a sum of Gaussian functions for the parameterization of the

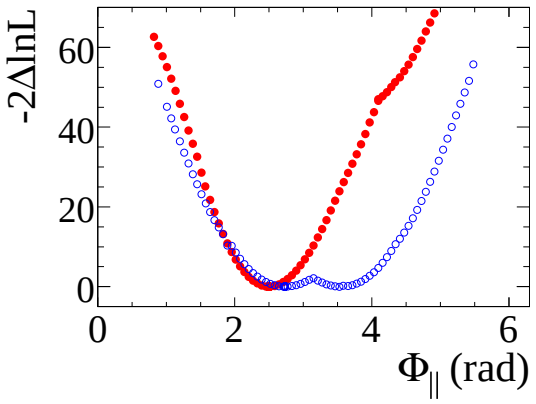

Figure 16: Distribution of $2\ln\mathcal{L}$ as a function of $\phi_\parallel$ for the two fit configurations: including P- and S-wave $K\pi$ interference into account (solid points) and ignoring it (open points). The former resolves the phase ambiguity.

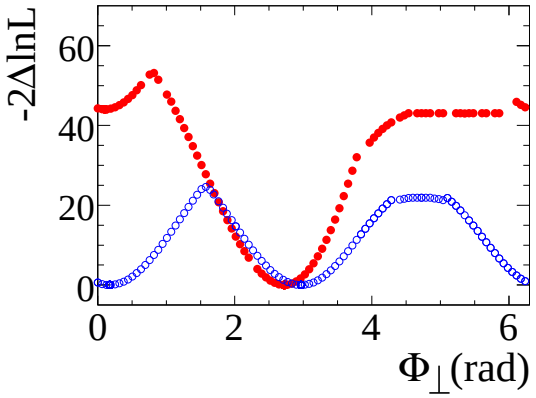

Figure 17: Distribution of $2\ln\mathcal{L}$ as a function of $\phi_\perp$ for the two fit configurations: including P- and S-wave $K\pi$ interference into account (solid points) and ignoring it (open points). The former resolves the phase ambiguity.

signal PDFs for ΔE, $m_{\rm ES}$, and $\mathcal{F}$. For the combinatorial background, we use polynomials, except for $m_{\rm ES}$ and $\mathcal{F}$ distributions which are parameterized by an empirical phase-space function and by Gaussian functions, respectively. Resonance production occurs in the background and is taken into account in the PDF.

4.2. Results

We observe a nonzero $B^\pm \to \varphi K^*(892)^\pm$ yield with significance, including systematic uncertainties, of more than 10σ. The significance is defined as the square root of the change in $2\ln\mathcal{L}$ when the yield is constrained to zero in the likelihood $\mathcal{L}$. In Table VI, results of the fit are presented, where the combined results are obtained from the simultaneous fit to the two decay subchannels.

We repeat the fit by varying the fixed parameters in $\boldsymbol{\xi}$ within their uncertainties and obtain the associated systematic uncertainties. We allow for a flavor-dependent acceptance function and reconstruction efficiency in the study of asymmetries. The biases from the finite resolution of the angle measurements, the dilution due to the presence of fake combinations, or other imperfections in the signal PDF model are estimated with MC simulation.

The nonresonant K^+K^- contribution under the φ is accounted for with the $B^0 \to f_0 K^{*0}$ category. Its yield is consistent with zero. The $m_{K\overline{K}}$ PDF shape in this category is varied from the resonant to phase-space and the yield is varied from the observed value to the extrapolation from the neutral B-decay mode [15] to estimate the systematic uncertainties. Additional systematic uncertainty originates from other potential B backgrounds, which we estimate can contribute at most a few events to the signal component. The systematic uncertainties in efficiencies are dominated by those in particle identification, track finding, and K^0_S and π^0 selection. Other systematic effects arise from event-selection criteria, φ and K^{*0} branching fractions, and the number of B mesons.

4.3. Discussion

The yield of the $\varphi(K\pi)^{*\pm}_0$ contribution is 57^{+14}_{-13} events with a statistical significance of 7.9σ, combining the $|A_{00}|^2$ term and the interference terms $2\mathcal{R}{\rm e}(A_{1\lambda}A^*_{00})$, which confirms the significant S-wave $K\pi$ contribution observed in the neutral B-decay mode [15]. The dependence of the interference on the $K\pi$ invariant mass [15, 20, 21] allows us to reject the other solution near $(2\pi-\phi_\parallel, \pi-\phi_\perp)$ relative to that in

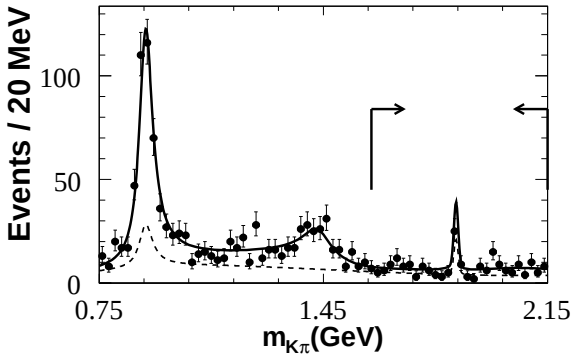

Figure 18: Distribution of the $K\pi$ invariant mass extended above 1.6 GeV from the study of $B^0 \to \phi(K^+\pi^-)$ decays in Ref. [15]. The data distribution is shown with a requirement to enhance the signal as discussed in regard to Fig. 14 in text. The solid (dashed) line shows the signal-plus-background (background) expected distributions. The arrows indicate the higher mass range, 1.60 to 2.15 GeV.

Table VII Summary of branching fraction ($\mathcal{B}$) and longitudinal polarization fraction (f_L) results for the various $B \to \varphi K^*$ decay on *BABAR*. The quantum numbers J^P are given for the K^* resonances. For a complete list of up to 12 independent parameters measured in the $\varphi K^*(892)^0$ and $\varphi K_2^*(1430)^0$ decay modes see Ref. [15].

J^P	B decay mode	$\mathcal{B}$ranching (10^{-6})	f_L
0^+	$\varphi K_0^*(1430)^0$	$4.6 \pm 0.7 \pm 0.6$	
1^-	$\varphi K^*(892)^0$	$9.2 \pm 0.7 \pm 0.6$	$0.51 \pm 0.04 \pm 0.02$
1^-	$\varphi K^*(892)^+$	$11.2 \pm 1.0 \pm 0.9$	$0.49 \pm 0.05 \pm 0.03$
1^-	$\varphi K^*(1680)^0$	$< 3.5 \quad (0.7^{+1.0}_{-0.7} \pm 1.1)$	–
2^+	$\varphi K_2^*(1430)^0$	$7.8 \pm 1.1 \pm 0.6$	$0.85^{+0.06}_{-0.07} \pm 0.04$
3^-	$\varphi K_3^*(1780)^0$	< 2.7 $(-0.9 \pm 1.4 \pm 1.1)$	–
4^+	$\varphi K_4^*(2045)^0$	$< 15.3 \quad (6.0^{+4.8}_{-4.0} \pm 4.1)$	–

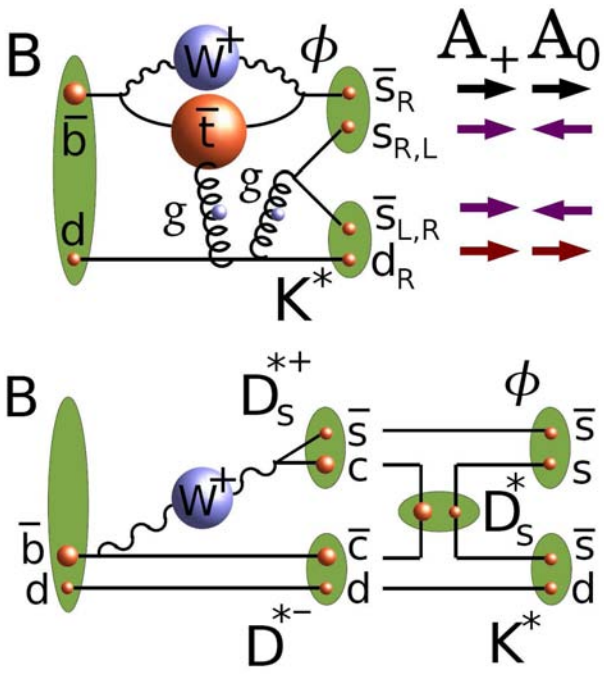

Figure 19: Feynman diagram describing the $B \to \varphi K^*$ decay with the new mechanisms within the standard model, such as annihilation penguin [18] (top) or QCD rescattering [19] (bottom).

Table VI with significance of 6.3σ, including systematic uncertainties. Figs. 16 and 17 illustrate resolution of the phase ambiguity.

The $(V-A)$ structure of the weak interactions, helicity conservation in strong interactions, and the s-quark spin flip suppression in the penguin decay diagram suggest $|A_{10}| \gg |A_{1+1}| \gg |A_{1-1}|$ [10]. This expectation disagrees with our observed value of f_L. We obtain the solution $\phi_\parallel \simeq \phi_\perp$ without discrete ambiguities, which is consistent with the approximate decay amplitude hierarchy $|A_{10}| \simeq |A_{1+1}| \gg |A_{1-1}|$.

We find that $\phi_\perp$ and $\phi_\parallel$ deviate from either π or zero by more than 3.1σ and 2.4σ, respectively, including systematic uncertainties. This indicates the presence of final-state interactions not accounted for in naive factorization. Our measurements of the six *CP*-violating parameters are consistent with zero and exclude a significant part of the physical region. We find no evidence of *CP* violation in this decay.

We have performed a full amplitude analysis and searched for *CP*-violation in the angular distribution of the $B^\pm \to \varphi K^{*\pm}$ decay. Our results are summarized in Table VI. Using similar techniques, we have also searched for the $B^0 \to \phi K^{*0}$ decays with the tensor $K_3^*(1780)^0$ and $K_4^*(2045)^0$, vector $K^*(1680)^0$, and scalar nonresonant $(K\pi)_0^{*0}$ contributions with $K^{*0} \to K^+\pi^-$ invariant mass above 1.6 GeV. Our results are summarized in Table VII. Fig. 18 shows distribution of the $K\pi$ invariant mass in this study. We do not find significant signal with the above resonances and place upper limits on the B-decay branching fractions.

These results find substantial A_{1+1} amplitude in the $B \to \varphi K^*(892)$ decay and point to physics outside the standard model as shown in Fig. 4 [17], where scalar interaction would look more consistent with the data, or new dynamics as shown in Fig. 19 [18, 19], where penguin annihilation is more consistent with sizable A_{1+1} and small A_{1-1}. Any satisfactory solution to this polarization puzzle is expected to explain all polarization data and to be predictive for other experimental measurements.

Acknowledgments

I am grateful for the work of my *BABAR* colleagues who made this contribution possible and for the excellent luminosity and machine conditions provided by our PEP-II colleagues. I would like to thank Guglielmo De Nardo and Steve Sekula for discussion of the $\tau\nu$ results, Zijin Guo and Yanyan Gao for discussion of the φK^* results, and the conference organizers for hospitality. This contribution was supported in part by the U.S. National Science Foundation and Alfred P. Sloan Foundation, and *BABAR* institutions are supported by the national funding agen-

cies.

References

[1] N. Cabbibo, Phys. Rev. Lett. **10**, 531 (1963).

[2] M. Kobayashi and T. Masakawa, Prog. Theor. Phys. **49**, 652 (1973).

[3] W. S. Hou, Phys. Rev. D **48**, 2342 (1993).

[4] G. Isidori and P. Paradisi, Phys. Lett. B **639**, 499 (2006).

[5] A. G. Akeroyd and C. H. Chen, Phys. Rev. D **75**, 075004 (2007).

[6] Particle Data Group, W.-M. Yao *et al.*, J. Phys. G33, 1 (2006).

[7] HPQCD Collaboration, A. Gray *et al.*, Phys. Rev. Lett. **95**, 212001 (2005).

[8] *BABAR* Collaboration, B. Aubert *et al.*, Phys. Rev. D **73**, 057101 (2006).

[9] K. Ikado *et al.*, Phys. Rev. Lett. **97**, 251802 (2006).

[10] A. Ali *et al.*, Z. Phys. C **1**, 269 (1979); G. Valencia, Phys. Rev. D **39**, 3339 (1989); G. Kramer and W.F. Palmer, Phys. Rev. D **45**, 193 (1992); H.-Y. Cheng and K.-C. Yang, Phys. Lett. B **511**, 40 (2001); C.-H. Chen *et al.*, Phys. Rev. D **66**, 054013 (2002); M. Suzuki, Phys. Rev. D **66**, 054018 (2002); A. Datta and D. London, Int. J. Mod. Phys. A **19**, 2505 (2004).

[11] *BABAR* Collaboration, B. Aubert *et al.*, presented at 1st International Workshop On Frontier Science: Charm, Beauty And CP, Frascati, Italy (October 2002); arXiv:hep-ex/0303020; Phys. Rev. Lett. **91**, 171802 (2003); **93**, 231804 (2004).

[12] Belle Collaboration, K.-F. Chen *et al.*, Phys. Rev. Lett. **91**, 201801 (2003); **94**, 221804 (2005).

[13] Belle Collaboration, J. Zhang *et al.*, Phys. Rev. Lett. **95**, 141801 (2005).

[14] *BABAR* Collaboration, B. Aubert *et al.*, Phys. Rev. Lett. **97**, 201801 (2006).

[15] *BABAR* Collaboration, B. Aubert *et al.*, Phys. Rev. Lett. **98**, 051801 (2007); arXiv:0705.0398 [hep-ex]; arXiv:0705.1798 [hep-ex].

[16] A. V. Gritsan and J. G. Smith, "Polarization in B Decays" review in [6], J. Phys. G33, 833 (2006).

[17] Y. Grossman, Int. J. Mod. Phys. A **19**, 907 (2004); E. Alvarez *et al.*, Phys. Rev. D **70**, 115014 (2004); P. K. Das and K. C. Yang, Phys. Rev. D **71**, 094002 (2005); C. H. Chen and C. Q. Geng, Phys. Rev. D **71**, 115004 (2005); Y. D. Yang *et al.*, Phys. Rev. D **72**, 015009 (2005); K. C. Yang, Phys. Rev. D **72**, 034009 (2005); S. Baek, Phys. Rev. D **72**, 094008 (2005); C. S. Huang *et al.*, Phys. Rev. D **73**, 034026 (2006); C. H. Chen and H. Hatanaka, Phys. Rev. D **73**, 075003 (2006); A. Faessler *et al.*, Phys. Rev. D **75**, 074029 (2007).

[18] A. L. Kagan, Phys. Lett. B **601**, 151 (2004); H. n. Li and S. Mishima, Phys. Rev. D **71**, 054025 (2005); C.-H. Chen et al., Phys. Rev. D **72**, 054011 (2005); M. Beneke *et al.*, Phys. Rev. Lett. **96**, 141801 (2006), arXiv:hep-ph/0612290; C.-H. Chen and C.-Q. Geng, Phys. Rev. D **75**, 054010 (2007); A. Datta *et al.*, arXiv:0705.3915 [hep-ph].

[19] C. W. Bauer *et al.*, Phys. Rev. D **70**, 054015 (2004); P. Colangelo *et al.*, Phys. Lett. B **597**, 291 (2004); M. Ladisa *et al.*, Phys. Rev. D **70**, 114025 (2004); H. Y. Cheng *et al.*, Phys. Rev. D **71**, 014030 (2005).

[20] LASS Collaboration, D. Aston *et al.*, Nucl. Phys. B **296**, 493 (1988); W. M. Dunwoodie, private communications.

[21] *BABAR* Collaboration, B. Aubert *et al.*, Phys. Rev. D **71**, 032005 (2005); Phys. Rev. D **72**, 072003 (2005).

[22] *BABAR* Collaboration, B. Aubert *et al.*, Nucl. Instrum. Methods **A479**, 1 (2002).

[23] S. Agostinelli *et al.*, Nucl. Instr. Meth. A **506**, 250 (2003).

[24] D. J. Lange, Nucl. Instrum. Methods **A462**, 152 (2001).

[25] Charge-conjugate modes are implied throughout the paper.

[26] E. Farhi, Phys. Rev. Lett. **39**, 1587 (1977).

[27] H. Albrecht *et al.* [ARGUS Collaboration], Phys. Lett. B **185**, 218 (1987).

[28] L. Lista, Nucl. Instrum. Methods **A462**, 152 (2001).

[29] A. L. Read, J. Phys. **G28**, 2693 (2002).

[30] *BABAR* Collaboration, B. Aubert *et al.*, arXiv:0705.1820 [hep-ex], Submitted to Phys. Rev. D.

[31] CKMfitter collaboration, J. Charles *et al.*, Eur. Phys. J. **C41**, 1 (2005); http://ckmfitter.in2p3.fr/

[32] *BABAR* Collaboration, B. Aubert *et al.*, Phys. Rev. D **70**, 032006 (2004).

[33] E791 Collaboration, E. M. Aitala *et al.*, Phys. Rev. Lett. **86**, 765 (2001).